Program Digest, 2019 IEEE International Ultrasonics Symposium (IUS)
Glasgow, Scotland, October 6-9, 2019

Improvement in Inclusion Contrast-to-Noise Ratio for Low-Displacement Acoustic Radiation Force (ARF) Elasticity Imaging Using a 3D Kernel Blind-Source Separation (BSS) Based Displacement Estimator

Md Murad Hossain*
Joint Department of Biomedical Engineering
University of North Carolina and North Carolina State University
Chapel Hill, NC, USA

Gabriela Torres
Joint Department of Biomedical Engineering
University of North Carolina and North Carolina State University
Chapel Hill, NC, USA

Caterina M. Gallippi
Joint Department of Biomedical Engineering
University of North Carolina and North Carolina State University
Chapel Hill, NC, US

Abstract— **Mechanical property assessment by elastographic ultrasound methods, including those that exploit acoustic radiation force (ARF), relies on accurate estimation of tissue displacement. Several displacement estimators have been developed, but their relevance to tracking ARF-induced displacements smaller than one micrometer is limited by estimation variance. To minimize displacement estimation variance, a new blind source separation (BSS)-based approach that exploits the spatial distribution of displacements is presented. This new approach applies principal component analysis (PCA) in three-dimensional (3D) kernels to derive dominant eigenvectors, from which displacements are estimated. We call this new approach the '3DK-BSS' estimator. The 3DK-BSS estimator is evaluated in terms of contrast-to-noise ratio (CNR) achieved in ARFI peak displacement (PD) images of a stiff (80 kPa) and a soft (8 kPa) spherical inclusion in a commercial phantom with a 25 kPA background. The CNR values achieved by 3DK-BSS were compared to those produced by normalized cross-correlation (NCC), Bayesian regularization, and BSS implemented using a two-dimensional (2D) kernel at ARF power levels of 5 to 45% of the full system power. For all power levels, and for both stiff and soft inclusions, 3DK-BSS inclusion CNR was higher than any other examined displacement estimator. For example, 3DK-BSS stiff inclusion CNR was 16.3, 11.8, and 4.2 times higher than the CNRs achieved by NCC, Bayesian regularization, and 2D BSS, respectively at 5% power level. CNR improvement by 3DK-BSS was largest at the lowest (5%) ARF power level, where displacement in the stiff phantom was measured by 3DK-BSS as 250 nm. These results suggest that, by accurately measuring sub-micrometer displacements, the 3DK-BSS displacement estimator could enable deeper ARF-based mechanical property assessments, finer mechanical resolution in stiff tissues, and/or lower ARF power requirements to expand the diagnostic relevance of ARF-based mechanical property assessments.**

Keywords—ARFI imaging, Blind Source Separation (BSS), displacement estimator, normalized cross-correlation, Bayesian Estimator.

I. INTRODUCTION

Over the past three decades, ultrasonic methods for interrogating the mechanical properties of tissues have been extensively studied and applied for the clinical diagnosis of diseases and injuries [1]. Such diagnostic applications have considered that the mechanical properties of tissue are related to their underlying structure and composition. Thus, alterations in structure and composition caused by disease or injury are detectable by evaluating tissue mechanical properties.

Among the various ultrasound approaches to interrogating tissue mechanical properties are those that exploit acoustic radiation force (ARF) [2]–[5]. An essential component to ARF-based mechanical property assessment is an accurate estimation of ARF-induced deformation, i.e., displacement, which is on the scale of micrometers. To estimate displacement from ultrasound data, several methods have been developed, including Kasai and Loupas motion estimators [6], which operate in the phase domain, and normalized cross-correlation (NCC), which operates in the time domain [6]. While these displacement estimators are generally well suited for measuring displacements of several micrometers, measurement variance can be as high as one micrometer or greater [7]. This degree of displacement variance limits interrogations of mechanical property in deep and/or very stiff tissue, where ARF-induced displacements may be less than one micrometer and set a lower bound on system power requirements.

Various methods for improving displacement estimation accuracy have been developed. For example, a Bayesian regularization approach that exploits information about the spatial distribution of displacement estimates has been demonstrated to achieve lower mean-square error for bulk displacement in strain-based elastography [8]. Also, a blind source separation (BSS)-based approach exploiting principal component analysis (PCA) was demonstrated to measure ARFI-induced displacement with lower variance than NCC [9]. Also using a PCA method, Hossain *et al.* detected nanometer-scale motion of super-paramagnetic iron oxide particles in magnetomotive ultrasound imaging [10] with prior knowledge of the frequency and phase of magnetic oscillations [11], [12]. These previous implementations of BSS-based displacement tracking brought estimation variance below that predicted by the Cramer-Roa lower bound [7], but further improvements might be achievable by exploiting two-dimensional (2D) spatial information.

* Md Murad Hossain is now a post-doctoral research scientist at Columbia University.

978-1-7281-4595-2/19/$31.00 ©2019 IEEE

The objective of this work is to incorporate 2D spatial information in BSS-based displacement tracking by performing PCA decompositions in three-dimensional (3D) (axial x lateral x time) kernels. This new approach, 3DK-BSS, is compared to NCC, Bayesian regularization, and BSS displacement estimation using a 2D (axial x time) kernel in terms of contrast-to-noise ratio (CNR) for delineating spherical inclusions in a commercially available elasticity phantom with low ARF power settings.

II. Methods

A. Phantom experiments

A calibrated cylindrical inclusion phantom (CIRS, Model 049A) was evaluated. The background Young's modulus was 25 kPa, and inclusions had Young's moduli of 80 kPa (stiff) or 8 kPa (soft). The inclusions were imaged in an elevation plain that achieved an inclusion cross-sectional diameter of 4.05 mm.

B. ARFI data acquisition and processing

ARFI imaging was performed using a Siemens S3000 Helix and a 9L4 transducer (Siemens Healthineers, Ultrasound Division, Issaquah, WA, USA) using the methods described in [13]. The employed ARFI beam sequence parameters are listed in Table 1. ARFI excitation pulse powers were varied from 5% to 45% of the full system power to induce different amounts of displacement. Acquired ARFI data sets were three-dimensional (axial x lateral x time).

C. Displacement estimation

ARF-induced displacement was estimated using NCC (1D axial kernel = 0.5 mm) [6], Bayesian regularization (1D axial kernel = 0.3 mm) [14], 2D BSS (1D axial kernel = 1.2 mm), and 3DK-BSS (axial kernel = 1.2 mm and lat kernel = 2.0 mm). The acquired raw RF data were made complex to enable separation of signal components based on the direction of motion, which was encoded in the phase component. For each (axial x lateral) pixel in the ARFI data volume, PCA was performed in a two-dimensional (axial x time) or a three-dimensional (axial x lateral x time) kernel surrounding the pixel. If the kernel was three-dimensional, the data was reformed into a 2D (axial*lateral x time) Casorati matrix [15]. Then, complex PCA was performed on the auto-correlation of the kernel data matrix. From the complex PCA decomposition, the principal (most energetic) eigenvector was identified. The phase of the most energetic eigenvector (v_1), sound speed (c, assumed to be 1540 ms^{-1}), and sampling frequency (f_s), were used to estimate the displacement (dx) as [9]:

$$dx = \frac{c}{2fs} \frac{\tan^{-1}\left(\frac{Im\,(v_1)}{Re(v_1)}\right)}{\tan^{-1}\left\{\frac{Im\left[\sum_{i=0}^{M-2}\sum_{j=0}^{N-1} K^*(i,j)K(i+1,j)\right]}{Re\left[\sum_{i=0}^{M-2}\sum_{j=0}^{N-1} K^*(i,j)K(i+1,j)\right]}\right\}}$$

Where K is 2D kernel data with size MxN.

D. Image Quality Metrics

Displacement estimator performance was compared in terms of inclusion contrast-to-noise ratio (CNR), using the equation,

Table 1 : ARFI beam squence parameters.

Name	Value
Transducer	9L4
Bandwidth	55.38%
Sampling freq.	40 MHz
Acoustic lens focus (axial, lateral, elevation)	(40, 0, 0) mm
ARF excitation duration	300 cycle
ARF excitation center frequency	4.0 MHz
ARF excitation F/#	1.5
ARF axial focus	34 mm
Tracking center frequency	6.0 MHz
Tracking transmit F/#	1.5
Tracking receive F/#*	0.75
Tracking transmit axial focus	34 mm
Tracking PRF	10 Hz
Tracking ensemble length	5 ms

*Aperture growth and dynamic Rx focusing enabled

$$CNR = \frac{|\mu_{inc} - \mu_{bkd}|}{\sqrt{\sigma_{inc}^2 + \sigma_{bkd}^2}}$$

where, μ and σ represent the median and standard deviation of displacement in the inclusion (inc) and background (bkd) regions of interest (ROI). The inclusion ROIs were circles centered on the inclusions and with a radius of 80% of the corresponding inclusions' radius. Background ROIs were rings surrounding the corresponding inclusions, with an inner radius of 120% and size same as inclusion's ROI.

III. Results and Discussion

Figure 1 (a and b) shows ARFI peak displacement (PD) in the 80 kPa inclusion and the 25 kPa background as estimated by NCC, Bayesian regularization, 2D BSS, and 3DK-BSS. The lowest detected displacement in the 80 kPa inclusion, which occurred with the ARF power set to 5%, was 250 nm. Panel (c and d) shows the coefficient of variation (COV = 100*standard deviation/mean) of PD in 80 kPa inclusion and the 25 kPa background for NCC, Bayesian regularization, 2D BSS, and 3DK-BSS. The coefficient of variation was lowest for 3DK BSS.

The impact of lower COV on ARFI imaging performance is apparent in the peak displacement images shown in Figure 2 (a). Visually, the stiff inclusion is more readily discerned by the two BSS displacement estimators than by the NCC or Bayesian regularization estimators. The further quantitative evaluation shows that inclusion CNR was 16.3, 11.8, and 4.2 times higher with the 3DK-BSS estimator than with NCC, Bayesian regularization, and 2D BSS estimators, respectively.

Figure 2(b-c) quantitatively compare inclusion CNR achieved using NCC, Bayesian regularization, 2D BSS, and 3DK-BSS displacement estimators for different ARF power levels in stiff (b) and soft (c) inclusions. Across all examined power levels, and for both stiff and soft inclusions, the 3DK-BSS displacement estimator yielded higher CNR than any of the

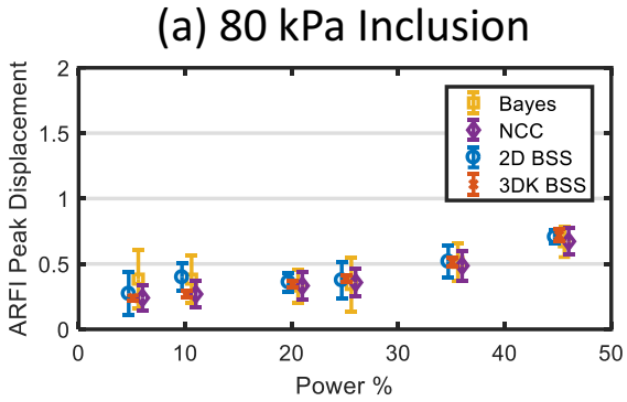

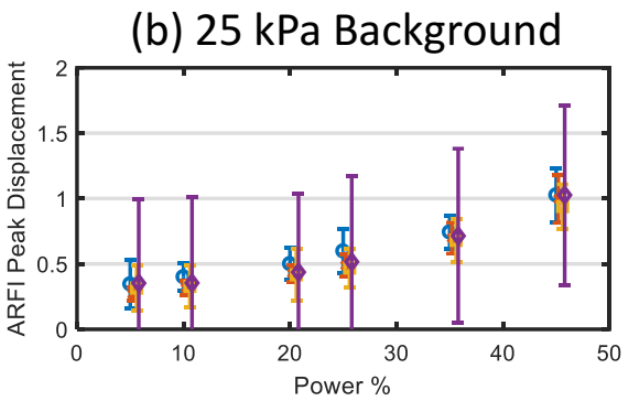

(c) 80 kPa Inclusion

Coefficient of Variation	Power (%)	5	10	20	25	35	45
	2D BSS	60%	27%	20%	36%	24%	7%
	3DK BSS	9%	9%	6%	7%	7%	6%
	Bayes	58%	48%	38%	60%	28%	18%
	NCC	39%	38%	32%	30%	23%	15%

(d) 25 kPa Background

Coefficient of Variations	Power (%)	5	10	20	25	35	45
	2D BSS	54%	27%	24%	28%	17%	20%
	3DK BSS	18%	18%	15%	17%	17%	18%
	Bayes	54%	48%	47%	32%	24%	18%
	NCC	182%	186%	137%	127%	93%	67%

Figure 1: ARFI peak displacement values of the inclusion (a), and background (b) of a calibrated phantom (CIRS 049A), for different ARF power levels. Values are calculated using NCC, Bayesian regularization, 2D BSS, and 3DK-BSS. Data are plotted as mean ± standard deviation of displacement in the ROI. The coefficient of variation (COV = 100*standard deviation/mean) of PD in inclusion (c) and in background (d) for NCC, Bayesian regularization, 2D BSS, and 3DK-BSS.

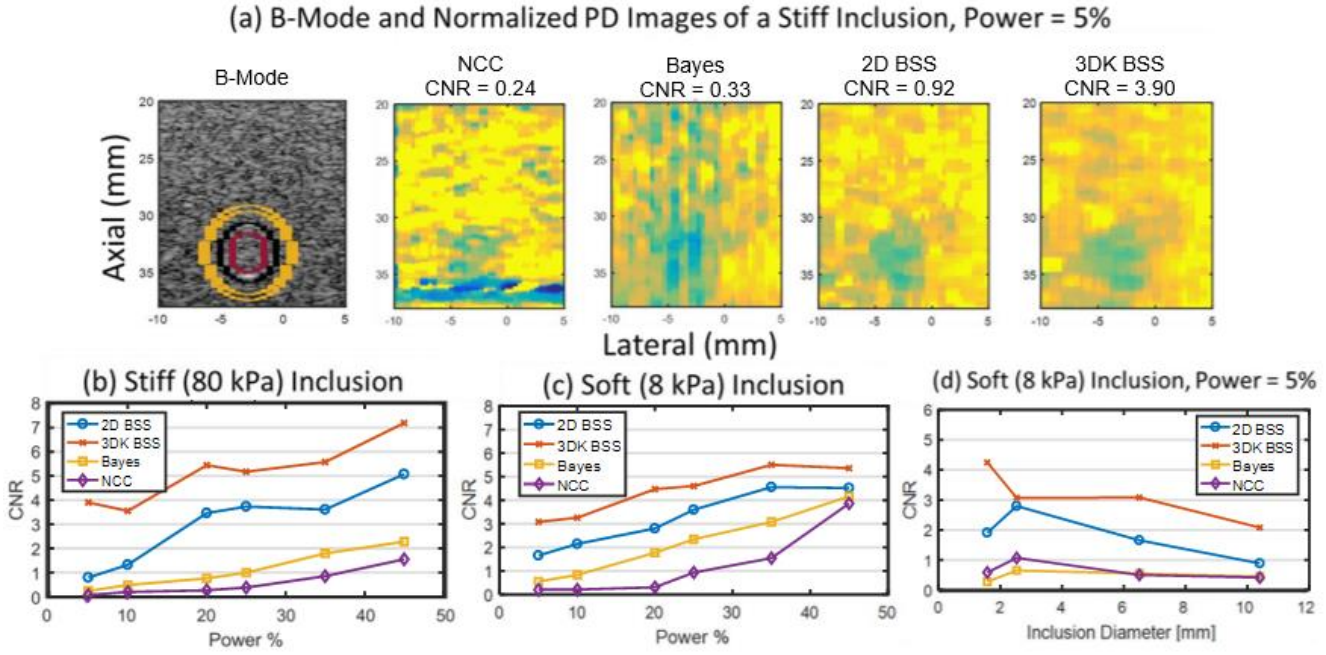

Figure 2: (a) Representative B-Mode and normalized peak displacement images by NCC, Bayesian regularization, 2D BSS, and 3DK-BSS estimators. The black indicates the true inclusion boundary, the red contour represents the inclusion ROI, and the space between the black and the yellow contours represents the background ROI for CNR calculation. Green and Yellow color in the normalized PD images represent lower (i.e., stiff) and higher (i.e., soft) displacement. (b) CNR derived using NCC, Bayesian regularization, 2D BSS, and 3DK-BSS displacement estimators in the (b) stiff and (c) soft inclusion as a function of ARF power level, expressed as a percentage of full system power.

other evaluated displacement estimators, with the biggest gain, achieved at the lowest (5%) ARF power level in the stiff inclusion.

IV. Conclusion

In this work, the 3DK-BSS displacement estimator was presented in the context of displacement tracking for ARFI imaging. The performance of the 3DK-BSS estimator was compared against that of the NCC, Bayesian regularization, and 2D BSS methods in terms of contrasting stiff and soft phantom inclusions using low ARF power levels. Inclusion CNR achieved by the 3DK-BSS displacement estimator was higher than that achieved using any other examined displacement estimator, especially for the smallest displacements. These results suggest that the 3DK-BSS displacement estimator could enable deeper applications of ARF-based mechanical property calculations, finer mechanical resolution in stiff tissues, and/or lower ARF power requirements to expand the overall diagnostic relevance of ARF mechanical property assessments.

Acknowledgment

The authors thank Siemens Healthineers, Ultrasound Division, Issaquah, WA, USA for in-kind support. This work was supported by NIH grants R01HL092944, R01NS074057, and R01DK107740.

References

[1] R. M. S. Sigrist, J. Liau, A. El Kaffas, M. C. Chammas, and J. K. Willmann, "Ultrasound Elastography: Review of Techniques and Clinical Applications," *Theranostics*, vol. 7, no. 5, pp. 1303–1329, 2017.

[2] K. Nightingale, S. McAleavey, and G. Trahey, "Shear-wave generation using acoustic radiation force: in vivo and ex vivo results.," *Ultrasound Med. Biol.*, vol. 29, no. 12, pp. 1715–1723, Dec. 2003.

[3] J. Bercoff, M. Tanter, and M. Fink, "Supersonic Shear Imaging : A New Technique," *IEEE Trans. Ultrason. Ferroelectr. Freq. Control*, vol. 51, no. 4, pp. 396–409, 2004.

[4] A. P. Sarvazyan, O. V. Rudenko, S. D. Swanson, J. B. Fowlkes, and S. Y. Emelianov, "Shear wave elasticity imaging: a new ultrasonic technology of medical diagnostics.," *Ultrasound Med. Biol.*, vol. 24, no. 9, pp. 1419–35, Nov. 1998.

[5] M. M. Hossain, T. Nichols, E. Merricks, and C. Gallippi, "Viscoelastic response (VisR)-derived relative elasticity and relative viscosity reflect tissue elasticity and viscosity: In silico and experimental demonstration in liver," in *2017 IEEE International Ultrasonics Symposium (IUS)*, 2017, no. 2, pp. 1–1.

[6] G. F. Pinton, J. J. Dahl, and G. E. Trahey, "Rapid tracking of small displacements with ultrasound.," *IEEE Trans. Ultrason. Ferroelectr. Freq. Control*, vol. 53, no. 6, pp. 1103–17, Jun. 2006.

[7] W. F. Walker and G. E. Trahey, "A Fundamental Limit on Delay Estimation Using Partially Correlated Speckle Signals," *IEEE Trans. Ultrason. Ferroelectr. Freq. Control*, vol. 42, no. 2, pp. 301–308, 1995.

[8] B. Byram, G. E. Trahey, and M. Palmeri, "Bayesian speckle tracking. Part II: biased ultrasound displacement estimation.," *IEEE Trans. Ultrason. Ferroelectr. Freq. Control*, vol. 60, no. 1, pp. 144–57, Jan. 2013.

[9] F. W. Mauldin, F. Viola, and W. F. Walker, "Complex principal components for robust motion estimation.," *IEEE Trans. Ultrason. Ferroelectr. Freq. Control*, vol. 57, no. 11, pp. 2437–49, Nov. 2010.

[10] B. E. Levy, M. M. Hossain, J. M. Sierchio, D. Thapa, C. M. Gallippi, and A. L. Oldenburg, "Effect of Model Thrombus Volume and Elastic Modulus on Magnetomotive Ultrasound Signal Under Pulsatile Flow.," *IEEE Trans. Ultrason. Ferroelectr. Freq. Control*, vol. 65, no. 8, pp. 1380–1388, Aug. 2018.

[11] M. Hossain, D. Thapa, J. Sierchio, A. Oldenburg, and C. Gallippi, "Blind source separation - based motion detector for sub-micrometer, periodic displacement in ultrasonic imaging," in *2016 IEEE International Ultrasonics Symposium (IUS)*, 2016, pp. 1–4.

[12] M. M. Hossain, B. E. Levy, D. Thapa, A. L. Oldenburg, and C. M. Gallippi, "Blind Source Separation-Based Motion Detector for Imaging Super-Paramagnetic Iron Oxide (SPIO) Particles in Magnetomotive Ultrasound Imaging.," *IEEE Trans. Med. Imaging*, vol. 37, no. 10, pp. 2356–2366, Oct. 2018.

[13] G. E. Trahey, M. L. Palmeri, R. C. Bentley, and K. R. Nightingale, "Acoustic radiation force impulse imaging of the mechanical properties of arteries: In vivo and ex vivo results," *Ultrasound Med. Biol.*, vol. 30, no. 9, pp. 1163–1171, 2004.

[14] D. Dumont and B. Byram, "Robust Tracking of Small Displacements with a Bayesian Estimator.," *IEEE Trans. Ultrason. Ferroelectr. Freq. Control*, Oct. 2015.

[15] C. Demené *et al.*, "Spatiotemporal Clutter Filtering of Ultrafast Ultrasound Data Highly Increases Doppler and fUltrasound Sensitivity," *IEEE Trans. Med. Imaging*, vol. 34, no. 11, pp. 2271–2285, 2015.